GLOBAL SOLAR TRANSMITTANCE OF VERTICAL GLAZINGS

Gerardo Vitale[1], Gonzalo Abal[1,2], Italo Bove[2], and Javier Pereyra[2]

[1] Solar Energy Lab, Physics Department, CENUR LN, Salto, (Uruguay)

[2] Solar Energy Lab, Physics Institute, Engineering School, Montevideo, (Uruguay)

Abstract

The thermal gain of glazings in buildings is usually modelled using concepts such as the solar factor (SF), the sum of the normal-incidence solar transmittance plus the ratio of the thermal energy emitted indoors to the incident solar irradiance. An important part of the SF of a vertical glazing is the visible solar transmittance which depends on the sky conditions and the relative amounts of beam and diffuse components of incident solar radiation. The directional transmittance of both components can be very different for large incidence angles. Using three years of 1-min measurements under outdoor conditions, this dependence is investigated and three global solar transmittance models are locally adjusted and evaluated. When the diffuse fraction of global solar radiation is measured, all models show good performance, with relative RMSD under 3% of the average transmittance and negligible bias. However, if the diffuse irradiance measurements are not available and it is estimated from locally adjusted diffuse fraction models, it is found that the rRMSD increases to 10% . This increase in accuracy is associated mostly with cloudy conditions.

Keywords: solar transmittance, transparent glazings, diffuse radiation

1. Introduction

The solar transmittance of transparent glazings is a key factor in determining the solar gain and thermal balance of a building. Usually the solar factor is used to characterize the thermal performance of a glazing. This factor is defined as the sum of the solar visible transmittance and a thermal transmittance term (Jelle, 2013) and it can be calculated from spectral transmittance and reflectivity measurements following standard methods (ISO9050, 2003). In this work we focus in the role of diffuse irradiance in the visible solar transmittance part of the solar factor.

The global solar irradiance incident on a given surface has a direct component, G_b, incident on the surface from the Sun's direction (with incidence angle θ) and a diffuse component, G_d, due to atmospheric scattering which has essentially no directional dependence. The global irradiance on the surface is the sum of both components, $G_i = G_b \cos\theta + G_{di}$. Under clear skies, about 15% of the irradiance is diffuse, but under cloudy conditions, 100% can be diffuse. The solar global transmittance τ_g of a transparent glazing is defined as

$$\tau_g = \frac{G_t}{G_i} \tag{1}$$

where G_t is the solar global irradiance transmitted by the glazing. Both G_i and G_t can be measured in W/m^2 using pyranometers and extend over the solar spectrum (wavelengths between 0.3 μm and 3 μm). Frequently, solar transmittance is modeled either as a constant factor which does not take into account the directional properties of the incident solar irradiance or as a directional beam (Duffie and Beckman 2006), which does not account properly for the diffuse component. Under partially cloudy skies (the most frequent condition in temperate climates), neither the directional model nor the constant transmittance models are fully adequate.

Uruguay's climate, with latitudes within 30-35° S, is classified as temperate with mostly hot summer or Cfa in the Köppen-Geiger climatic classification scheme (Peel et al., 2007). More than half of the daylight hours correspond to skies with partial cloud cover. In a previous work (Vitale et al., 2018), we considered the global transmittance of horizontal glazings in order to study the transmittance dependence on the diffuse component of solar irradiance in a simpler context, in which the radiation reflected from neighbouring surfaces can be neglected. In this paper, the more relevant case of vertical glazings is considered. A framework in which beam transmittance models can be combined with diffuse transmittance to obtain the global transmittance of a vertical

transparent material is proposed. Three directional transmittance models are adjusted and experimentally evaluated within this framework. The seasonal variation in the average albedo of neighbouring surfaces is obtained from the irradiance measurements and taken into account. Finally, the impact of modeling (instead of measuring) the diffuse component of the incident solar irradiance is also assessed.

1.1 Framework for combining transmittance models

If an isotropic distribution for diffuse irradiance is assumed, the incident global irradiance on a vertical glazing is (Duffie and Beckman 2006)

$$G_i = G_{bi} + G_{di} = G_b \cos\theta + \frac{1}{2}\left(G_{dh} + \rho G_h\right) \tag{2}$$

where G_h is the horizontal global irradiance, G_{dh} is the diffuse component and ρ is the ground albedo for diffuse reflection. The scheme in Fig. 1 illustrates the geometry of the situation.

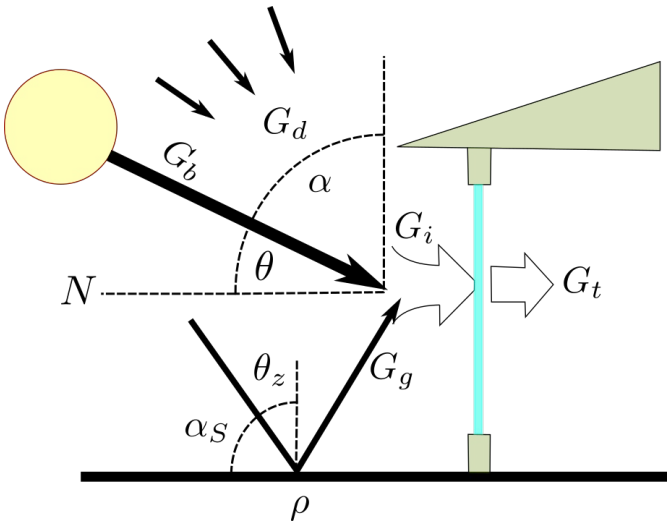

Fig. 1. Scheme showing the components of solar irradiance relevant to transmittance in a vertical glazing. In this context, "sky radiation" is a synonim of diffuse irradiance. Adapted from Marion and Wilcox, 1995.

The solar irradiance transmitted by a vertical glazing comes in part from beam irradiance and in part from diffuse irradiance. Different transmittances apply, mainly due to the directional properties of the former. Beam and diffuse transmittances can be defined as $\tau_b = G_{bt}/G_{bi}$ and $\tau_g = G_{dt}/G_{di}$, respectively, see Eq. (2) for the incident components. The global irradiance transmitted by the vertical glazing is

$$G_t = \tau_b\, G_b \cos\theta + \frac{\tau_d}{2}\left(G_{dh} + \rho G_h\right). \tag{3}$$

As a result, the global transmittance in Eq. (1) can be expressed as the weighted average of the beam and diffuse transmittances,

$$\tau_g = \mu\tau_b + (1-\mu)\tau_d \quad \text{with} \quad \mu = \frac{(1-f_d)\, r_b}{(1-f_d)\, r_b + \frac{1}{2}\left(f_d + \rho\right)} \tag{4}$$

where the weighting factor is expressed in terms of $r_b = \cos\theta/\cos\theta_z$ (see Fig. 1, for a visualization of the incidence angles) and the diffuse fraction $f_d = G_{dh}/G_h$. For a horizontal surface, the weight is simply $\mu = 1 - f_d$ (Vitale et al., 2018).

The isotropic model is simple, but systematically underestimates solar irradiance on a tilted surface because it does not consider the anisotropic distribution of diffuse irradiance in the sky. A more accurate model is that of Hay and Davies, which deals with the anisotropic distribution of diffuse irradiance in an effective way by treating a portion of circumsolar irradiance as directional beam irradiance (Hay and McKay, 1985). In practice, the use of this model reduces to using a modified diffuse fraction $\tilde{f}_d$ in Eq. (4), defined as

$$\tilde{f}_d = f_d(1 - T_b) \quad \text{with} \quad T_b = (1 - f_d)k_T \tag{5}$$

where $T_b = G_b/G_0$ is the atmospheric solar beam transmittance. It can be expressed in terms of the diffuse fraction f_d and the clearness index $k_T = G_h/G_0 \cos\theta_z$, where G_0 is the solar irradiance at the top of the atmosphere (i.e. the conventional solar constant 1367 W/m^2 corrected by the orbital variation in Sun-Earth distance), see (Duffie and Beckman 2006) for details. In sum, the modified diffuse fraction, Eq. (5) is used in Eq. (4), and this implies that the improved anisotropic transport model of Hay and Davies is being used.

Eq. (4) combines the directional (beam) transmittance properties with the isotropic (diffuse) transmittance taking into account the proportion of diffuse irradiance, as indicated by the diffuse fraction. Irradiance reflected from the ground can be a relevant contribution to the diffuse irradiance incident on a vertical glazing. It is included in Eq. (4) with the dependence on the ground reflectivity (albedo) parameter ρ. This is a meta-model for solar transmittance, in which transmittance models with directional properties can be used for τ_b and diffuse fraction models (Abal et al., 2017) can be used to obtain f_d from global horizontal irradiance, when its diffuse component is not measured.

1.2 Directional transmittance models

The first model to be considered is a physical model for directional transmittance, which we label DB for easy reference. It is based on Snell's law and Fresnel's relations, as described in (Duffie and Beckman 2006). Beam transmittance can approximately be expressed as a product $\tau_b = \tau_a \tau_r$ in which τ_a accounts for the loss due to absorption in the glazing material and τ_r represents the losses due to reflection. The absortion-related transmittance is obtained from the Lambert-Beer-Bouguer law as,

$$\tau_a = \exp(-KL/\cos\theta') \quad \text{with} \quad \theta' = \arcsin(\sin\theta/n) \tag{6}$$

where L is the thickness of the glazing, K is the optical extinction coefficient of the material and θ' is the angle of the refracted beam in the glazing, obtained from Snell's law in terms of the incidence angle and the index of refraction n of the glazing. For unpolarized sunlight, transmittance across a semi-transparent refracting glazing can be expressed as,

$$\tau_r = \frac{1}{2}\left(\frac{1-r_\parallel}{1+r_\parallel} + \frac{1-r_\perp}{1+r_\perp}\right) \quad \text{with} \quad r_\parallel = \frac{\tan^2(\theta'-\theta)}{\tan^2(\theta'+\theta)} \quad \text{and} \quad r_\perp = \frac{\sin^2(\theta'-\theta)}{\sin^2(\theta'+\theta)} \tag{7}$$

where $r_\parallel$ and $r_\perp$ are the reflectances for the parallel and perpendicular polarization components of the beam respectively, obtained from the Fresnel relations. Taking into account multiple reflections within the glazing, the directional transmittance from the DB model can be expressed as

DB: $$\tau_b(\theta) = \frac{\tau_a}{2}\left[\frac{(1-r_\parallel)^2}{1-(r_\parallel\tau_a)^2} + \frac{(1-r_\perp)^2}{1-(r_\perp\tau_a)^2}\right]. \tag{8}$$

Assuming that the index of refraction is known from specification sheets (or can be independently measured as in this work), the only parameter in the DB model is the optical thickness of the glazing, KL. At normal incidence, Eq. (8) reduces to

$$\tau_b(0) = \tau_n = e^{-KL} \times \left[\frac{(1-r_n)^2}{1-(r_n e^{-KL})^2}\right] \quad \text{with} \quad r_n = (n-1)^2/(n+1)^2. \tag{9}$$

Thus, within this physical model, the normal incidence beam transmittance, τ_n, is determined by the value of the parameters n and KL. This physical model is the basis of the solar transmittance calculation implemented in the popular simulation software Energy Plus (Crawley, 2001; Winkelmann, 2001).

The second model, labeled ISO, is a simple parametrization for beam transmittance used in the ISO9806 standard for testing solar collectors (ISO9806, 2013),

ISO: $$\tau_b(\theta) = \tau_n\left[1 - b_0\left(\frac{1}{\cos\theta} - 1\right)\right] \tag{10}$$

where b_0 is an adjustable dimensionless parameter.

The third model considered, SS, is a simple parametrization initially proposed as a substitute for global

transmittance in a simulation software (Schultz and Svendsen, 1998),

SS: $$\tau_b(\theta) = \tau_n \left[1 - \tan^p(\theta/2)\right] \quad (11)$$

where p is a dimensionless parameter which depends on the glazing (p=4 for float glass). This model turns out to be useful for modeling global transmittance in composite semi-transparent surfaces, such as polycarbonate sheets.

1.3 Diffuse transmittance

Diffuse transmittance on a vertical glazing results from the incident diffuse radiation from the sky and surrounding surfaces (considered as perfect diffuse reflectors). Diffuse irradiance has no directional dependence and the diffuse transmittance is independent of the incidence direction. In actual practice, each situation must be analized carefully as there may be nearby surfaces with some specular reflection (i.e. white metallic surfaces or large bodies of still water), but the basic model assumes an isotropic distribution of diffuse irradiance in the hemisphere defined by the surface. Brandemuehl and Beckman originally calculated the diffuse transmittance under the isotropic hypotheses and concluded that it can be expressed easily by using expressions for beam transmittance at an effective angle θ_e that depends on the receiving surface tilt angle β. For horizontal or vertical receiving surfaces, the effective angle is approximately $\theta_e = 60^o$ (Brandemuehl and Beckman 1980). In sum, for vertical glazings, diffuse transmittance τ_d can be modeled as having the constant value

$$\tau_d = \tau_b(\theta = 60^o). \quad (12)$$

For each directional transmittance model considered, both transmittances, τ_b and τ_d, are combined according to Eq. (4) to produce the global transmittance of the glazing.

2. Measurements and Results

The three transmittance models presented in Section 1 are adjusted and tested against data for a real vertical glazing with the Sun as light source.

2.1 Experimental facility

The experimental setup was located at the Solar Energy Laboratory at Salto, Uruguay (latitude = 31.28° S, longitude = 57.92° W, altitude = 56 m above sea level). The glazing sample was common window float glass with an average thickness (measured at several points) L = 5.90 ± 0.05 mm. It was located on a vertical plane, at ground level, facing North. Two Licor 200R solar radiometers were mounted on a vertical plane one of them behind the glazing and the other in front of it, as shown in Fig. 2a. These instruments measure the global irradiances G_i and G_t from which the global transmittance τ_g is calculated using Eq (1). They where calibrated before and after the measurement period, against a secondary standard (Kipp & Zonen CMP22 pyranometer) with trazability to the World Radiometric Reference (WRR) at PMOD, Davos. The Licor instruments were chosen because of their fast response time and their better performance under inclined conditions compared with dome-equipped pyranometers. Data was recorded at every minute, using a Fischer Scientific DT85 data acquisition system. At a distance of 20 m, from the vertical glazing, a precision solar tracking system (Kipp & Zonen, SOLYS2) was fitted with two CHP1 pyrheliometers, two CMP11 pyranometers and one Licor 200R sensor. One of the pyranometers was shaded by a ball assembly to measure the diffuse horizontal irradiance, G_{dh}. The other two provide the global horizontal irradiance G_h and the pyrheliometers measure the direct normal irradiance, G_b. Measurements are recorded at every minute by another Fischer Scientific DT85 data acquisition system. These instruments are calibrated every two years following the ISO 9847:1992 standard against the above mentioned secondary standard (Kipp & Zonen CMP22) normally kept in storage at the Solar Energy Lab. A minute-based dataset for the solar irradiance variables G_h, G_b, G_{bh}, G_i and G_t was assembled for this work. Additionally, the usual meteorological variables (ambient temperature, atmospheric pressure, wind direction and speed, relative humidity) are recorded every minute by a research-grade meteorological station located less than 100 m from the main setup.

2.2 Laboratory characterization of the glazing

A sample of the float glass was tested under laboratory conditions to determine its optical properties. Normal incidence optical spectral transmittance was measured for wavelengths between 0.3 − 2.5 μm. For the UV-

Visible region, a 150 W Xe lamp (Newport 96000) was used as a source of optical excitation (solar simulator). The signals were coupled into an Ocean Optics spectrometer (FLAME-S-UV-VIS) by a 50 μm optical fiber also from Ocean Optics. For the Visible-NIR characterization, a tungsten lamp was used as a source of excitation, the light was chopped with a SRS SR540 chopper and coupled into a monochromator (Oriel 77250 with a 77299 grating). The transmitted light was detected with an InGaAs thermo-cooled photodiode (Newport 71586). Finally, the signal was measured with a lock-in amplifier (SRS 530 Stanford Research Systems). For the IR region the same lamp was used, but after chopped, the light was coupled into a Newport cornerstone 260 extended-range monochromator. The transmitted light was measured with a thermocooled InAs photodiode from Sciencetech and the signal was detected by the Lock-in amplifier. The resulting spectral transmittance is shown in Fig. 3.

(a) (b)

Fig. 2. Setup used for solar measurements. (a) Two Licor 200R pyranometers are mounted on the vertical plane, facing North, parallel to the vertical glazing (float glass). Behind the glass there are a few Platinum RTD temperature sensors, since the setup is part of a Trömbe wall facility made with Adobe bricks. (b) SOLYS2 precision solar tracker with ventilated measurements of direct normal, diffuse and global horizontal solar irradiances.

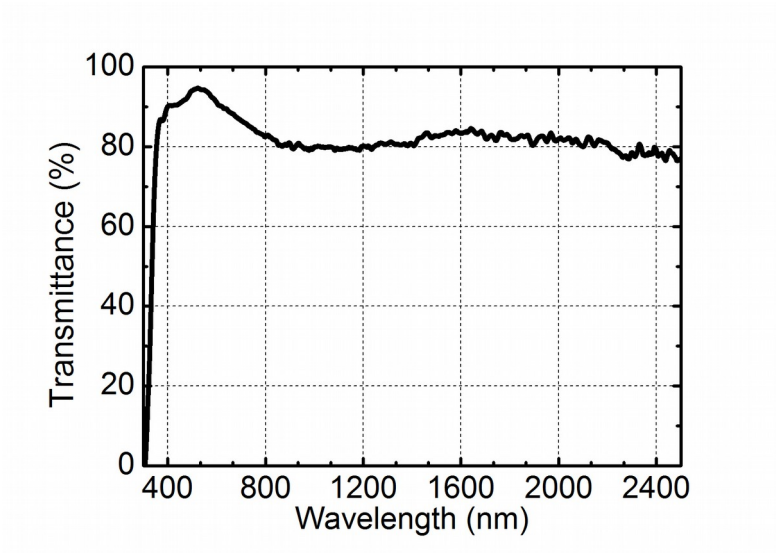

Fig. 3. The black curve shows the spectral transmittance T(λ) of a sample of float glass (under normal incidence) measured under laboratory conditions for the solar spectrum range (0.3 − 2.5 μm.) .

The total beam transmittance of the sample was calculated from the measured spectral transmittance T(λ) using the AM 1.5 standard solar spectra G-173-03 (ASTM 2012) as follows

$$\tau_n = \frac{\int_{0.3}^{2.5} T(\lambda)\, G_s(\lambda)\, d\lambda}{\int_{0.3}^{2.5} G_s(\lambda)\, d\lambda} = 0.855 \tag{13}$$

The index of refraction of the glass sample was determined (using a red laser with λ=633 nm and a precision goniometer) to be n = 1.53 ± 0.01.

2.3 Ground albedo determination

Frequently, in the absence of more reliable information, an ad-hoc value is chosen for the reflection coefficient of the ground (albedo), ρ, which appears in Eqs. (2) and (4). For instance, in (Marion and Wilcox, 2995) a value of ρ = 0.20 is used to generate all the information and the value recommended in (Hunn y Calafell, 1977) for grass ranges between 0.2 and 0.3. The ground surrounding our experimental setup is composed of a small wooden deck and an area of grass. A seasonal effect in the albedo, due to the different pigmentation of the grass between summer and winter can be expected.

Since we had several years of simultaneous measurements of global irradiance on the vertical (G_i) and horizontal (G_h) planes and the diffuse fraction f_d was also measured, the average reflectivity could be determined from Eq. (2) using linear regression. An overall average reflectivity (albedo) of ρ = 0.32 was obtained and the seasonal behaviour shown in Fig. 4 emerges when the data is separated by month. The solar reflectivity of the surrounding grass varies significantly (between 0.25 and 0.42), being lower in Summer (December-February) and higher in Winter (June-July).

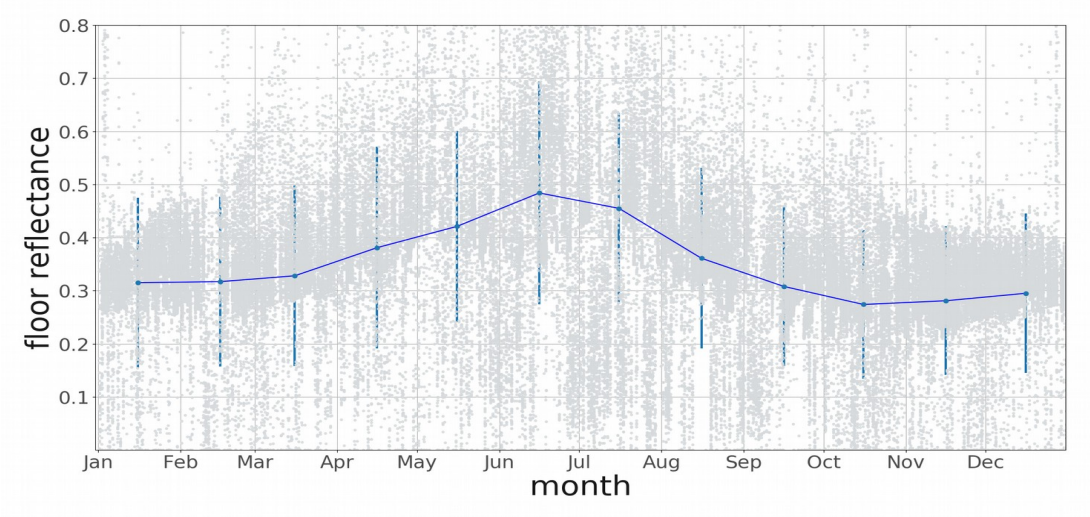

Fig.4 Mean albedo or ground reflectivity at the experimental facility for each month of the year. Gray dots are estimated from the data. The blue line is a linear interpolation of the monthly averages (the bars correspond to ± one std. deviation).

2.4 Methodology and data filtering

As mentioned, global solar irradiances were measured and recorded at each minute. However, for this work, the 1-minute solar irradiance database was integrated to 5 minute averages in order to minimize the effect of short-lived, over-irradiance events due to transient cloud reflections. The resulting 129020 daytime records of 5-min data where filtered following to the recommendations of the Baseline Solar Radiation Network - BSRN (Long and Dutton, 2002). Three additional filters where applied in order to remove data points affected by conditions such as low Sun or large incidence angles, associated to large experimental uncertainties:

i) low Sun: $\alpha_s > 5^o$ or $\cos\theta_z > 0.087$

ii) transmittance: $0.10 < \tau_g < 1$

iii) incidence angle on glazing: $\alpha > 8^o$ or $\theta < 82^o$

After these filters are applied, a set of 30113 5-min records with valid τ_g and f_d are obtained and these form the basis for the adjustment and evaluation of the transmittance models. Half of the data set is selected randomly as the "training set" for adjusting the model parameters (as described below) and the other half is used as the "evaluation set". For each record, the incidence angle is computed and Eqs. (6-11) are used to obtain the beam and diffuse solar transmittances for each model and using Eq. (4) the estimated global transmittances are obtained. The modified diffuse fraction from Eq. (5) is used to include anisotropy in the transport model (effectively using Hay and Davies transport model), although this step is not essential.

The models are evaluated using the standard Mean Bias Deviation (MBD) and Root Mean Square Deviation (RMSD) indicators. For a set of N measurements y_i and estimates $\hat{y}_i$ they are defined by,

$$MBD = \frac{1}{N}\sum_{i=1}^{N}(\hat{y}_i - y_i) \quad \text{and} \quad RMBD = \left[\frac{1}{N}\sum_{i=1}^{N}(\hat{y}_i - y_i)^2\right]^{\frac{1}{2}} \tag{15}$$

and they can be expressed in relative terms, as a percentage, relative to the average of the measured values.

Tab. 1. Parameters for each transmittance model. KL, τ_n and b_0 are fitted by multiple linear regression to the transmittance data, the index of refraction n is measured in the lab and p is fixed at 4 for float glass. The diffuse transmittance was calculated from Eq. (12).

model for τ_g	**normal global transmittance (τ_n)**	**diffuse transmittance (τ_d)**	**parameters**
DB, Eqs (8) and (4)	0.800	0.711	KL = 0.136; n = 1.53
ISO, Eqs (9) and (4)	0.803	0.714	b_0 = 0.109
SS, Eqs. (10) and (4)	0.795	0.706	p = 4

For each model, the free parameters (either KL or τ_n and b_0) are adjusted to the adjustment dataset by standard multiple linear regression. Table 1 shows the results of the adjustment and derived parameters, such as diffuse transmittance, from Eq. (12). The index of refraction was measured indoors as described in Section 2.3. These results show that the normal beam transmittances obtained from the three models are consistent and

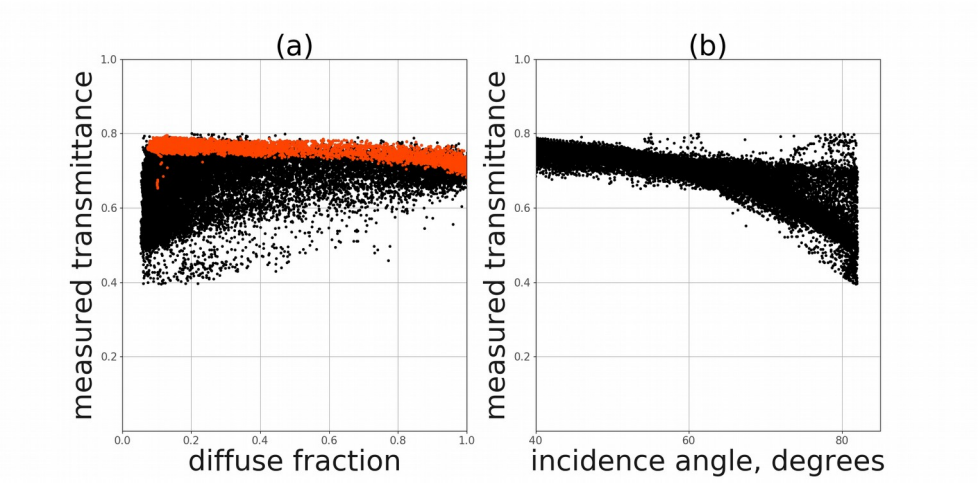

Fig. 5. Measured transmittance. (a) Transmittance vs diffuse fraction (the red dots correspond to incidence angles under 45°).

(b) Transmittance vs incidence angle

τ_n = 0.80 for this sample under solar light in average outdoor conditions. Laboratory measurements made for a standard solar spectrum with a specific airmass (AM = 1.5) result in a higher normal transmittance (0.855). The

outdoor experimental conditions include air masses up to 11.5 and a mix of cloudy and clear-sky conditions, therefore different solar spectra are involved. About 37% of the data records correspond to mostly clear-sky conditions, 60% to mixed cloudiness and less than 3 % to total cloud cover. The diffuse transmittances obtained from Eq. (12) are also consistent between models, with $\tau_d = 0.71$. Fig. 5 shows the measured global transmittance as a function of (a) diffuse fraction and (b) incidence angle. Under clear-sky conditions *($f_d < 0.2$)* a range of transmittances between 0.3 and 0.8 are obtained, depending on the air mass. Under cloudy conditions *($f_d = 1$)* the global transmittance is approximately 0.70 with a small spread.

3. Results

A scatter plot for the SS model estimates (global transmittance vs the measured values) is shown in Fig. 6 (upper panel). The lower panels show the global transmittance as function of the incidence angle, as predicted by each model against the filtered dataset in the background. The three models follow the decreasing trend of beam transmittance with incidence angle (relevant under clear-sky conditions) correctly and produce similar results for diffuse transmittance under cloudy conditions. A quantitative assessment is made using the evaluation dataset and the indicators defined in Eq. (15). The results for each model, are expressed in relative terms as a % of the average of the measured global transmittance,$\langle\tau_g\rangle = 0.691$, and they are shown in Table 2.

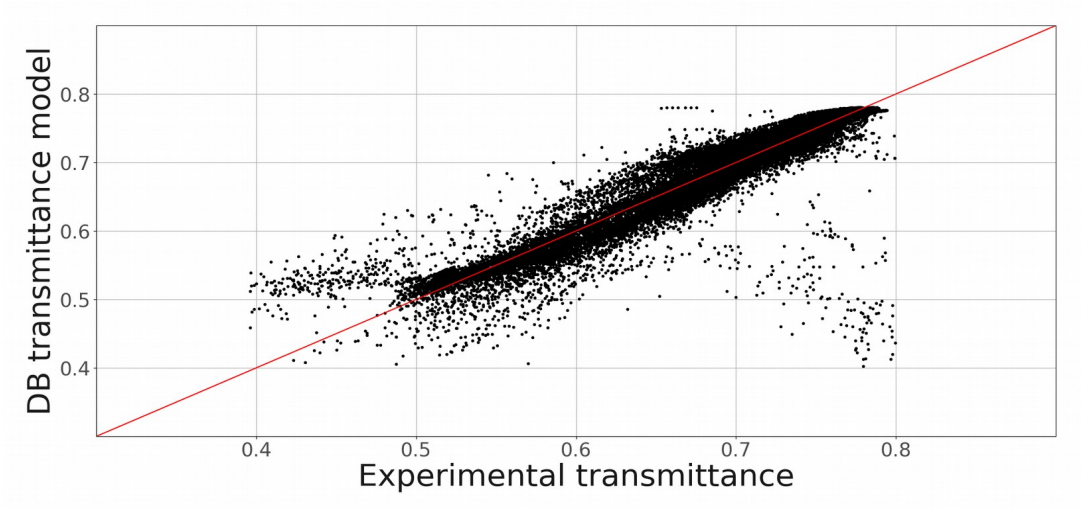

Fig. 6. Scatter plot for modeled transmittance vs measured transmittance for the SS model.

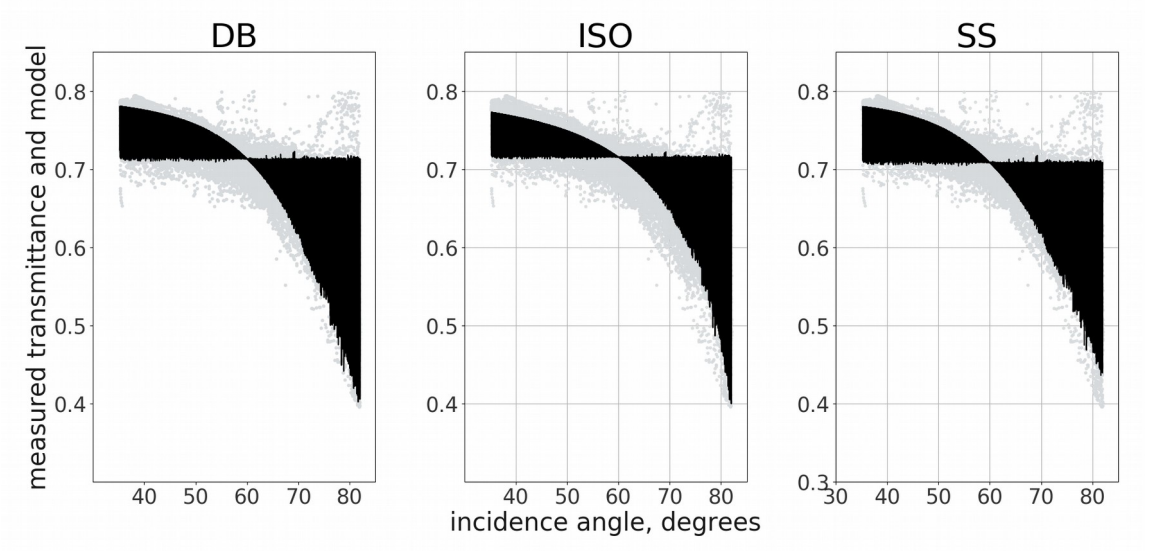

Fig. 7. Dependence of global transmittance with incidence angle. Models in black, data represented by gray dots.

All models perform well when combined in Eq. (4) under all-sky conditions with an average rRMSD of 2.9 % and small biases. When analyzed under clear-sky, partially cloudy or full cloudiness conditions, the rRMSD indicators increases only slightly (to an average of 3.3 % across models) under partial cloudiness (worst case) and biases remain under ±1% in all cases.

In order to use Eq. (4), the diffuse fraction must be known and diffuse irradiance is not an easily available variable for the average user of transmittance models. An estimate of the diffuse fraction can be obtained from global horizontal irradiance using phenomenological separation models (Abal et al, 2017) and its interesting to assess the impact of estimating the diffuse fraction on the performance indicators of the transmittance models.

The analysis in (Abal et al, 2017) considered ten models for diffuse fraction and evaluated their performance using solar irradiance data for the territory of Uruguay. Taking into account simplicity and performance, one of the best models is the one proposed in (Ruiz-Arias et al. 2010), based on a double exponential function

$$f_d = a_0 + a_1 e^{-\exp(a_2 + a_3 k_t + a_5 m)} \tag{16}$$

where the air mass m can be approximated by $m = 1/\cos\theta_z$, unless θ_z is close to 90^0 (sunrise or sunset conditions) in which case a corrected expression must be used. The localized version of this model, RA2s, using the parameters a_i as listed in Table 10 of (Abal et al, 2017) estimates the diffuse fraction with an rRMSD under 20% of the measured mean of f_d in the region of interest in this work. The indicators obtained from the transmittance models when the diffuse fraction is estimated from global irradiance using Eq. (16) is shown in the two rightmost columns of Table 2 (marked in gray). Small biases (under 2 %) appear, and the rRMSD

Tab. 2. Indicators for the three global transmittance models expressed as a % of the mean value of the measured global transmittance $\langle\tau_g\rangle = 0.691$

model for τ_g	measured difuse fraction		modeled difuse fraction	
	rMBD (%)	rRMSD (%)	rMBD (%)	rRMSD (%)
DB, Eqs (8) and (4)	0.0	2.8	-0.7	10.1
ISO, Eqs (9) and (4)	1.2	3.0	2.3	10.4
SS, Eqs. (10) and (4)	0.0	2.9	1.5	10.3

Tab. 3. Indicators for the three global transmittance models with modeled diffuse fraction separated by sky condition, expressed as a % of the mean value of the measured global transmittance $\langle\tau_g\rangle = 0.691$.

	clear sky		partial clouds		full cloud cover	
model for τ_g	rMBD	rRMSD	rMBD	rRMSD	rMBD	rRMSD
DB	-2.5	3.6	-0.6	12.7	7.7	15.8
ISO	1.0	3.5	2.5	12.9	10.6	17.5
SS	0.0	3.2	1.6	12.9	9.5	16.9

indicators increase from 3.3 % to an average of 10.3 % across models. This may be acceptable, depending on the desired application. In Table 3, these results are resolved for the different sky conditions. There are large positive biases (between 7 and 11%) under full cloud cover, indicating considerable transmittance overestimation by all models in this condition. A large difference appears in the rRMSD indicator, which increases only slightly under clear-sky conditions but becomes large (between 13-17%) under cloudy skies. This reflects a weakness of most diffuse fraction models, which are known to perform worst under partial cloudiness conditions (Abal et al., 2017). However, in the conditions in which models perform worst (under cloudiness), the transmitted energy flux should also be small. Under clear-sky conditions, when the energy flux is expected to be large, the transmittance models are accurate, even if the diffuse fraction is calculated.

4. Conclusions

This paper focuses on models for the solar transmittance of vertical glazings under real outdoor conditions. It is shown experimentally that properties of incident solar irradiance such as the incidence angle or the diffuse component (determined mainly by cloudiness) have a relevant impact on solar transmittance of a vertical glazing and can decrease it by more than 60% with respect to the normal-incidence, clear-sky value.

A theoretical framework is proposed to incorporate a dependence of the global transmittance on the diffuse component of the incident radiation (diffuse fraction). Solar irradiance (incident and transmitted) measurements were made, at 1-minute intervals, during a three-year period on a vertical glazing made of 6 mm thick float glass. The two components (beam and diffuse) of horizontal solar irradiance were also measured using a precision solar tracker and quality-controlled instruments. All data was filtered according to well established quality control procedures. Three beam transmittance models were locally adjusted and assessed in their ability to predict global solar transmittance under all-sky conditions. They perform similarly and accurately under all sky conditions (rRMSD under 3% with negligible bias) if the diffuse irradiance component is measured. The beam normal and the diffuse transmittances found by fitting all models to the data was 80 % and 71% respectively. And these results are consistent across the three models.

The effect on the solar transmittance models of using an estimated diffuse fraction from a locally adjusted separation model has also been evaluated. It was found that this increases the rRMSD from 3% to 10 %, on average under all-sky conditions. When these results are desaggregated for different sky conditions, it becomes clear that the main impact due to the use of a separation model takes place under cloudy conditions when rRMSD can reach 17% with large biases. Since the main energy exchange occurs under clear skies, and in this case the impact on all transmittance models is small, the methodology may be useful in energy efficiency applications in buildings. The best model for directional transmittance, based on simplicity and good performance, is the SS model even though it was initially formulated for global transmittance (Schultz, J.M. and S. Svendsen, 1998) . It has a single adjustable parameter and can potentially describe the solar transmittance of other kind of transparent materials with internal structure, such as polycarbonates or corrugated plastics, commonly used in buildings. This aspects will be investigated in a future work.

5. Aknowledgements.

The authors thank Dr. Daniel Ariosa, from the Physics Institute, Facultad de Ingeniería, UDELAR (Uruguay), for his help in the determination of the index of refraction of the transparent glazing sample used for this work.

6. References

Abal, G., Aicardi, D., Alonso-Suárez, R. and Laguarda, A. (2017). Performance of empirical models for diffuse fraction in Uruguay, Solar Energy, 141 166-181.

ASTM G173-03 (2012), Standard Tables for Reference Solar Spectral Irradiances, ASTM International, West Conshohocken, PA, https://www.astm.org/Standards/G173.htm

Brandemuehl, M.J. and Beckman, W.A. (1980). Transmission of diffuse radiation through CPC and flat plate collector glazings, Solar Energy 24, pp. 511–513.

Crawley, D.B. et al. (2001). Energy Plus: Creating a new-generation building energy simulation program, Energy and Buildings, 33, pp. 319-331.

Duffie, J.A. and Beckman W.A. (2006). Solar Engineering of Thermal Processes. Third ed. Hoboken, New Jersey: Wiley and Sons. ISBN : 978-0-471-69867-8.

Hay, J.E. and McKay, D.C. (1985). Estimating solar irradiance on inclined surfaces: A review and assessment of methodologies. Int. J. Solar Energy, 3, 203.

Hunn, B. y Calafell, D. (1977). Determination of average ground reflectivity for solar collectors. Solar Energy, 19:87.

Jelle, B. P. (2013), Solar radiation glazing factors for window panes, glass structures and electrochromic windows in buildings—Measurement and calculation, Solar Energy Materials & Solar Cells 116, 291–323.

ISO Technical Committee (2013). Solar test methods for solar thermal collectors. ISO standard 9806:2013(E). International Organization for Standarization http://www.iso.org/iso.

ISO Technical Committee (2003). Glass in building — Determination of light transmittance, solar direct transmittance, total solar energy transmittance, ultraviolet transmittance and related glazing factors. ISO standard 9050:2003(E). International Organization for Standarization http://www.iso.org/iso.

Long, C. N. and Dutton, E. G. (2002). BSRN Global Network recommended QC tests, V2.0, BSRN Technical Report, hdl:10013/epic.38770.d001.

Marion, W. and Wilcox, S. (1995). Solar Radiation Data Manual for Buildings, NREL Tech. Report N RELITP-463-7904, September 1995, https://rredc.nrel.gov/solar/pubs/bluebook/

Peel, M. C., Finlayson, B. L., Mcmahon, T. A., (2007). Updated world map of the Köppen-Geiger climate classification. Hydr. Earth-Sys. Sci. Disc., Europ. Geosc. Un., 11, 1633-1644.

Ruiz-Arias, J.A. et al., 2010. Proposal of a regressive model for the hourly diffuse solar radiation under all-sky conditions. Energy Conversion and Management 5, 881–893.

Schultz, J.M. and S. Svendsen (1998). Winsim: A simple simulation program for evaluating the influence of windows on heating demand. Solar Energy 68, 251–258.

Vitale, G., Bove, I. Abal, G., (2018). Transmitancia solar de coberturas vidriadas: el rol de la radiación difusa. Anais do VII Cong. Brasil. de Energia Solar (CBENS) – Gramado, 17-20 abril 2018, ISBN: 978-85-62179-02-0, URL: les.edu.uy/investigacion/

Winkelmann, F.C., (2001). Modeling windows in Energy Plus, presented at Seventh International IBPSA Conference, Rio de Janeiro, Brazil August 13-15, 2001. Building Simulation, pp. 457-464.